journal homepage: http://www.elsevier.com/locate/jmbbm

Adhesion of spider cribellate silk enhanced in high humidity by mechanical plasticization of the underlying fiber

Dakota Piorkowski [a], Chen-Pan Liao [a,b], Anna-Christin Joel [c,d], Chung-Lin Wu [e], Niall Doran [f], Sean J. Blamires [g], Nicola M. Pugno [h,i], I-Min Tso [a,j,*]

[a] Department of Life Science, Tunghai University, Taichung, 40704, Taiwan [b] Department of Biology, National Museum of Natural Science, Taichung, Taiwan [c] Department of Biological Sciences, Macquarie University, Sydney, Australia [d] Institute of Biology II, RWTH Aachen University, Aachen, Germany [e] Center for Measurement Standards, Industrial Technology Research Institute, Hsinchu, Taiwan [f] Bookend Trust, Hobart, Tasmania, Australia [g] Evolution and Ecology Research Centre, University of New South Wales, Sydney, NSW, Australia [h] Laboratory of Bio-Inspired Bionic, Nano Meta Materials & Mechanics, Department of Civil, Environmental and Mechanical Engineering, University of Trento, Via Mesiano 77, I-38123, Trento, Italy [i] School of Engineering and Materials Science, Queen Mary University, Mile End Rd, London, E1 4NS, UK [j] Center for Tropical Ecology and Biodiversity, Tunghai University, Taichung, Taiwan

ARTICLEINFO

Keywords:
Silk
Spider
Adhesion
Biological material

ABSTRACT

The disruptive nature of water presents a significant challenge when designing synthetic adhesives that maintain functionality in wet conditions. However, many animal adhesives can withstand high humidity or underwater conditions, and some are even enhanced by them. An understudied mechanism in such systems is the influence of material plasticization by water to induce adhesive work through deformation. Cribellate silk is a dry adhesive used by particular spiders to capture moving prey. It presents as a candidate for testing the water plasticization model as it can remain functional at high humidity despite lacking an aqueous component. We performed herein tensile and adhesion tests on cribellate threads from the spider, *Hickmania troglodytes*; a spider that lives within wet cave environments. We found that the work of adhesion of its cribellate threads increased as the axial fibre deformed during pull-off experiments. This effect was enhanced when the silk was wetted and as spider body size increased. Dry threads on the other hand were stiff with low adhesion. We rationalized our experiments by a series of scaling law models. We concluded that these cribellate threads operate best when the nanofibrils and axial fibers both contribute to adhesion. Design of future synthetic materials could draw inspiration from how water facilitates, rather than diminishes, cribellate silk adhesion.

1. Introduction

For many synthetic resins, glues and epoxies, exposure to water or high humidity often reduces adhesive strength (Ito et al., 2005; Lee, 2013). Water reduces the glass transition temperature (T_G) of many polymeric materials causing plasticization. Water-induced plasticization is typically mechanically characterized by a decrease in elastic modulus, and thermal stability (Marom, 1985), which has also been observed in many natural polymers, such as spider silk (Plaza et al., 2006). For some synthetic adhesives, water sorption may have catastrophic consequences due to swelling stresses, formation of micro-cracks or polymer chain degradation from hydrolytic cleavage (Marom, 1985; Wolff, 1993; Musto et al., 2002). Thus, designing synthetic adhesives with intended uses in wet conditions, such as underwater, moist environments (e.g. within the wet tropics or caves) or in vivo, presents a major engineering challenge (Bascom, 1974). Therefore, observations of natural adhesives, such as spider capture silk that exploits the presence of water, may be used to inspire the development of novel synthetic materials (Wolff et al., 2017).

Many web-building spiders produce silk capture threads used to immobilize fast moving prey in aerial traps (Eberhard, 1990; Blackledge et al., 2011). In general, these composite threads are composed of strong
underlying silk fibers surrounded by an adhesive material, which may be an aqueous glue (in the case of viscid silk) or sticky nanofibrils (in the case of cribellate silk) (Blackledge et al., 2011). In viscid silk threads, mechanical plasticization of the underlying silk fibers by water stored in the glue has been shown to increase compliance and extensibility (Vollrath and Edmonds, 1989; Perea et al., 2013). This allows for greater energy dissipation during adhesion as forces are effectively transferred from the glue to the fiber (Opell and Hendricks, 2007; Sahni et al., 2011). Unlike many synthetic adhesives, mechanical performance, such as breaking stress and toughness, is not greatly diminished and even enhanced by water, which allows for improved work of adhesion (Vollrath and Edmonds, 1989; Opell and Hendricks, 2007; Perea et al., 2013). Water also plays an important role in generating interfacial adhesion as it both stabilizes and spreads the adhesive glycoproteins (Sahni et al., 2014). As mechanical plasticization of the underlying fiber and interfacial adhesion cannot occur without the presence of water,

decoupling these effects has proven difficult. Studies examining the effects of mechanical plasticization on capture thread adhesion have, therefore, relied on theoretical modeling rather than empirical testing (Guo et al., 2018). Spider cribellate capture silk may prove a better model for empirically testing this effect, as it is a dry adhesive, so it does not necessarily rely upon water for adhesion.

Cribellate threads are complex materials that vary in form across the spiders that use them in webs (Eberhard and Pereira, 1993). There are, however, two common features across all of the cribellate silk using spiders. Firstly, the underlying axial fibers (diameter: 1–2 μm) that are always extruded from pseudoflagelliform spinnerets and provide support for the entire cribellate thread (Eberhard and Pereira, 1993). Secondly, hundreds of sticky cribellate nanofibrils (diameter: 10–100 nm) are produced in a plate-like spinneret and meticulously combed into a puffy shroud using a specialized structure on the spider's leg called the calamistrum (Kovoor, 1987; Eberhard and Pereira, 1993; Joel et al., 2015). Cribellate silk threads are functional in low and high humidity conditions, including tropical and sub-tropical forests, at night, near streams, and in caves (Eberhard and Pereira, 1993; Hawthorn & Opell, 2002, 2003).

The cribellate nanofibrils generate adhesion through van der Waals forces, physical entanglement and interaction with substrate micro- features (Hawthorn & Opell, 2002, 2003; Bott et al., 2017). Studies have postulated the presence of electrostatic charges inducing adhesive attraction with insect cuticle (Eberhard, 1988; Kronenberger and Vollrath, 2015). However, recent work suggests cribellate nanofibrils behave like dipoles (Joel and Baumgartner, 2017). At high humidity (99% RH) cribellate threads can generate greater adhesive forces than low humidity (2%RH) (Hawthorn & Opell, 2002, 2003), which have been attributed to the presence of hygroscopic forces, i.e. capillary action (Hawthorn and Opell, 2003).

There has been some debate in the literature over the effect of water on cribellate silk adhesive performance, particularly in relation to methods used (Joel and Baumgartner, 2017). Several studies that generated high humidity through evaporated air found increased adhesive performance (Hawthorn & Opell, 2002, 2003). However, when high humidity is generated using the fine mist of a nebulizer, adhesion is dramatically reduced as the puffy structure of the cribellate nanofibril shroud collapses and becomes matted (Liao et al., 2011; Elettro et al., 2015; Joel and Baumgartner, 2017). High moisture content, i.e. exposure to liquid water droplets, may be a reason for the disparate results from these studies and could cause the damaging effects (Joel and Baumgartner, 2017). However, most studies investigating the influence of water upon cribellate threads have mostly focused on cribellate nanofibrils and have largely overlooked the underlying axial fiber.

The axial silk fibers of cribellate silk have been assumed too stiff (Young's modulus = ~5 GPa) to deform significantly by the relatively low adhesive forces generated by the cribellate nanofibrils (30–60 μN) (Hawthorn and Opell, 2003; Blackledge and Hayashi, 2006a). This has led to the belief that the majority of the work of adhesion by cribellate threads can be attributed to the swaths of cribellate nanofibrils with the axial fibers providing little to no contribution to adhesion (Sahni et al., 2011). However, much of this work has been conducted at ambient conditions or low humidity that would mask the plasticizing effects of water on the underlying axial silk fiber. Recent work demonstrated that at humidity of 90% RH or greater, generated by evaporated water, axial fiber modulus decreases by an order of magnitude in cribellate threads from uloborid spiders (Piorkowski and Blackledge, 2017), indicating axial fibers can be subjected to water-induced mechanical plasticization.

The Tasmanian cave spider *Hickmania troglodytes* (Araneae: Austrochilidae, Fig. 1) (Higgins and Petterd, 1883) uses cribellate capture threads in wet cave environments that are consistently at 100% RH (Doran et al., 1999; Piorkowski et al., 2018a). We hypothesized that increased compliance of the cribellate axial fiber through plasticization by water increases the capacity for cribellate threads to do adhesive work in this species. These spiders grow slowly and there is a variety of different sized individuals in any one cave at any one time. We accordingly examined whether body size further contributed to cribellate silk adhesion.

2. Methods & materials

2.1. Field collection of webs

We collected fragments of wild webs from 24 *H. troglodytes* individuals (body lengths: 6 mm–22 mm, see Table S1) within wooden, circular frames (area = 310 cm^2; diameter = 19.8 cm,see Piorkowski et al., 2018a for details) in the caves of Southwest National Park, Tasmania, Australia (21 total) for mechanical testing and the wet forest of Mt. Wellington, Tasmania (3 total) for SEM/TEM imaging. The webs were identified visually and collected under natural tension. Prior to collecting the web fragments spiders were captured and their body length (cephalothorax + abdomen) measured to the nearest 0.5 mm using calipers. The purpose of measuring body length was to correlate it with spider growth, as per Piorkowski et al. (2018a). The frames containing webs were enclosed in protective film and transported under controlled conditions (~20 °C, ~35% RH) to Tunghai University, Taichuing, Taiwan (21 total) and RWTH Aachen University, Aachen, Germany (3 total), as it was not possible to transport samples at the same humidity within the wet cave or forest. While we cannot completely disregard any possible effects of drying and later re-wetting, cribellate silk does not have an aqueous component like other nature adhesives and is likely not significantly damaged by drying.

2.2. Laboratory collection of silk threads

From each web fragment we collected at least two cribellate silk threads for tensile testing and another two for adhesion (for a total of 90 silk samples from 21 spiders) with an additional 8 cribellate threads from 6 individuals were used for contraction testing. Webs were visually inspected for damage or accidental strain after transportation and only regions of web that remained pristine were sampled. Threads were easily identifiable within the web fragments because of their light blue hue (Lopardo et al., 2004). Individual silk threads were collected on 20 × 13 mm paper strips with a 10 × 10 mm gap cut out of the edge forming a U-shaped frame, as described by Piorkowski et al. (2018a). Double-sided sticky tape was affixed to the thin edges of the U-shaped frame. We carefully extracted taut cribellate threads by adhering them to the sticky tape and then cutting the thread from the web section with scissors. Samples that were damaged, strained or did not adhere to the sticky tape were discarded. We applied Elmer's ® glue atop the silk sample to ensure strong adhesion between the frame and silk and reduce the risk of the silk sample sliding off the frame during testing, as done in previous studies (Piorkowski et al., 2018a).

Additional silk threads (n = 3) were used to test for any structural change in cribellate silk threads when exposed to high humidity (>90%

Fig. 1. Tasmanian cave spider, *Hickmania troglodytes*, in its web (a), and a polarized light image of a cribellate capture thread at 100x magnification (b). Axial fibers (1, arrows) are visible in the center of the thread and the faint shroud of cribellate fibrils (2, surrounding axial fiber). For image in panel (a): Copyright: SIXTEEN

LEGS/Bookend Trust, Photograph credit: Joe Shemesh.

RH) and collected over 0.7 cm gaps between two twisted zinc paper clips using double-sided sticky tape. Samples were stored in the dark and protected from dust at room temperature and humidity (~20^{O}C and 45% RH) in a microscope slide box. Due to contamination (minute dust particles, prey remnants, etc.) from field collection all samples were examined thoroughly and only the most pristine threads were used for imaging.

2.3. Imaging nanofibril response to high humidity

Cribellate silk threads were observed with SEM/TEM before and after exposure to high humidity. Thread samples were placed into a sealed glass chamber with dishes filled with saturated KNO_3 solution to adjust the relative humidity of the chamber to about 95% at room temperature. They were stored at high humidity for a week and their shape was observed through the glass via light microscopy. This experiment was repeated three times. Afterwards threads were prepared for electron microscopy. For scanning electron microscopy (REM 525 M; Philips AG), threads were positioned between two strips of conductive foil with a gap of approximately 2 mm to avoid distortion from accidental attachment of the thread to the surface of the sample holder, which would change their structure. Threads were observed native, i.e. without any coating, using a spot size of about 40 nm, 15 kV and a SE- detector. We never observed a difference in thread diameter for any cribellate thread when comparing light and scanning electron microscopy, if the thread was uncoated. Coating can nonetheless change the diameter of silk threads (compare to Joel and Baumgartner, 2017). For transmission electron microscopy (TEM 10; Carl Zeiss) to further characterize the cribellate nanofibrils, thread samples were transferred to finder-grids (Plano GmbH). The cribellate nanofibrils are sensitive to the electron beam and tend to align themselves with each other. However, we did not see visible differences between treatments exposed to different humidity levels so we inferred that our method of humidification does not have a damaging effect on the morphology of the cribellate threads or on their adhesive properties (Fig. 2).

2.4. Adhesion testing and videography

Adhesion testing was done using a Nano Bionix ® tensile tester (MTS Systems Corp., Eden Prairie, MN, USA) at the Center for Measurement Standard of the Industrial Technology Research Institute in Hsinchu, Taiwan within 2.5 weeks of collection of threads in the field. We tested the adhesive properties of cribellate threads from 20 *H. troglodytes* individuals in wet (>90% RH) and dry (ambient laboratory conditions, 45% RH) conditions. High humidity was generated through exposure to evaporated water as it does not cause adverse structural changes (Hawthorn & Opell 2002, 2003; Joel and Baumgartner, 2017), see above, which have been attributed to high humidity generated using a nebulizer (Liao et al., 2011; Elettro et al., 2015). Evaporated water was pumped into a sealed Perspex chamber at a flow rate of 7 l/min. The chamber was not used for tests conducted in dry conditions as these were the ambient conditions of the testing facility. We tested two samples, one in each condition, from the same individual for as many individuals as possible (N = 14). However, samples from some individuals were only tested in wet (N = 2) or dry (N = 4) conditions. Each thread sample was tested 2–3 times for a total of n = 46 tests in wet conditions and n = 53 tests in dry conditions (see Table S2).

Silk thread fragments were mounted above and perpendicular to a force plate on the extension arm of the tensile tester. We mounted a stainless steel stage (4 mm × 2 mm) onto the force plate to serve as the
substrate for attachment. Threads were lowered onto the stage and held at a tension of 7 μN for 20 s to ensure firm contact. Each thread was then slowly pulled off the stage at an extension rate of 0.1 mm s^{-1} (See Fig. 3 and Movie S1 & S2 for images and video of pull-off tests).

We generated load-extension curves as the thread detached from the stage, from which we determined the: i) force at detachment (F_D), as the load at detachment, ii) the thread extension at detachment, as the vertical distance traveled by the crosshead of the tensile tester from the start of testing (after 20 s of tension, see above) to the point of detachment and iii) work of adhesion (W_D), as the area under the load-extension curve. For repeat tests of the same sample, the extension arm crosshead was slightly shifted after each test to allow a fresh segment of the silk thread to come in contact with a different region of the steel stage. Samples were allowed to relax for 30 s before the next test. Adhesive performance slightly decreased after each test as the cribellate nanofibril structure was often damaged or warped (see Results).

We used a Nikon D500 digital camera (30 fps) with a Laowa 60 mm f2.8 macro lens to capture video of adhesion tests for a single silk thread in both 45% RH and 90% RH conditions. Since the chamber we used was transparent, we were able to focus the camera through it.

2.5. Diameter measurement & tensile testing

All samples were observed to contain two disjoined axial fibers with surrounding cribellar fibrils (Fig. 1). Prior to tensile testing, we used polarized light microscopy (Blackledge et al., 2005) to obtain images of both axial fibers, as they were sometimes in separate planes of view. Samples were mounted atop an unused silk collecting frame to prevent the sticky cribellate fibrils from adhering to the glass stage of our microscope. We made three measurements of diameter

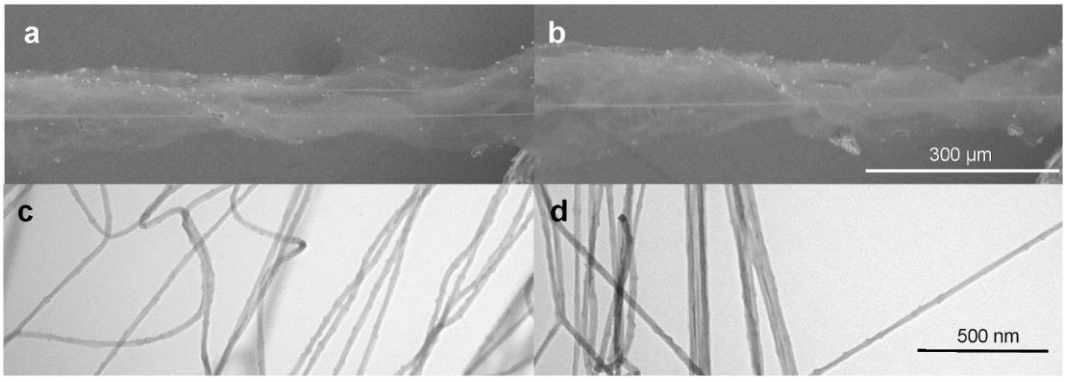

Fig. 2. Scanning electron microscopy (SEM) images (a–b) and transmission electron microscopy (TEM) images (c–d) of *H. troglodytes* cribellate capture silk taken at 45% RH (a,c) and 95% RH (b,d). Images were taken from two silk samples, for each imaging method, from the same individual. Samples were first stored at low humidity before imaging, then exposed to high humidity for one week before imaging a second time.

per axial fiber using ImageJ software (ver. 1.51r) and found a mean value across the six measurements.

Cross-sectional area for threads was calculated as:

$$A = 2\pi(d/2)^2$$

where *d* is mean axial fiber diameter. We did not measure diameters for cribellar fibrils as they are too fine to be accurately determined with our methods and have been shown to contribute marginally to the resistance of loading during tensile testing while the thicker, stronger axial fibers are still intact (Blackledge and Hayashi, 2006a).

We determined the quasi-static tensile properties of *H. troglodytes* cribellate silk from 64 individual thread fragments of 19 individual spiders using the same facilities and conditions as used for adhesion testing. We exposed 29 silk samples to dry environmental conditions (45% RH, 23°C) and 35 samples to wet conditions (>90% RH, 23°C) for 2–3 min directly prior to testing. We tested two samples from the same individual, one in each condition, for as many individuals as possible (N = 14). However, samples from some individuals were only tested in wet (N = 4) or dry (N = 1) conditions.

We generated force-extension data of silk threads mounted vertically and parallel to the tensile tester's highly sensitive force plate (accuracy to ~100 nN) pulled to breaking (strain rate = 1.5% s^{-1}). We calculated engineering values for stress and strain ("true" values also included in Table S3). Engineering strain was calculated as:

$$\varepsilon_E = (L_F - L_0)/L_0$$

where L_F is the final gauge length of the silk thread and L_0 is the original length.

We calculate engineering stress as:

$$\sigma_E = F/A_0$$

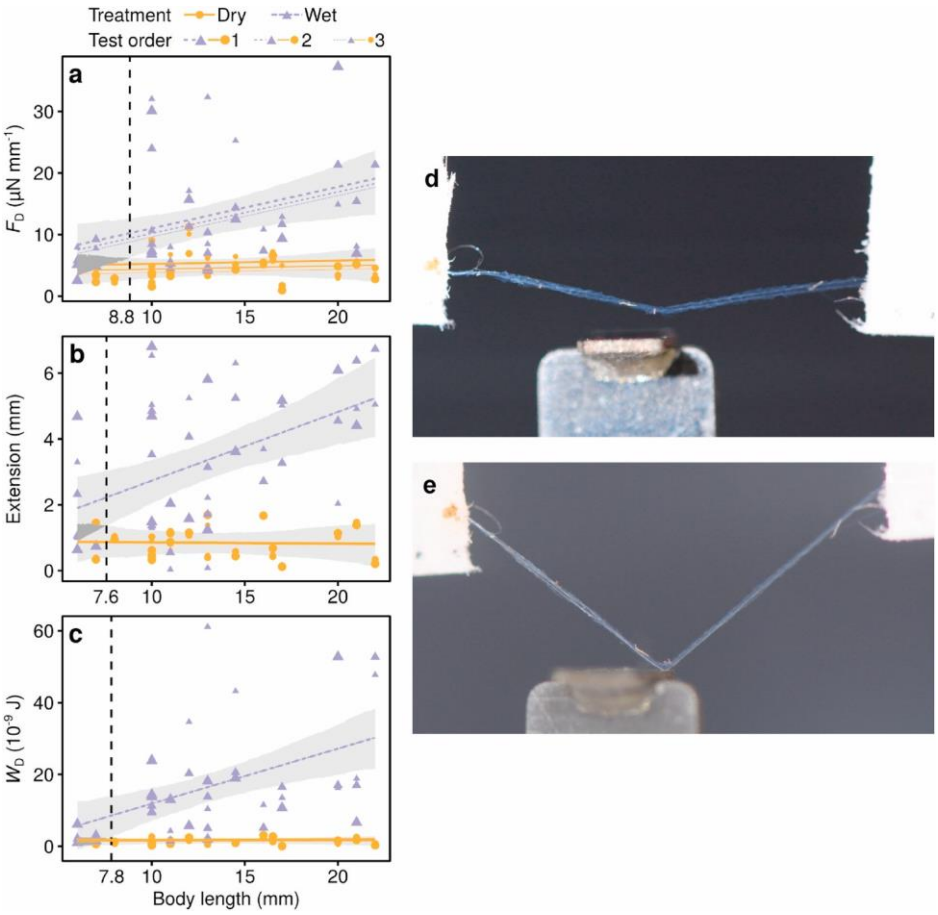

Fig. 3. Adhesive properties of force at detachment (F_D) (a), extension at detachment (b), and work of adhesion (W_A) (c) of cribellate silks of *H. troglodytes* in relation to body length and exposure treatment (Dry: 45% RH, Wet: 90% RH) with representative images of adhesive behavior in dry (d) and wet (e) conditions. Individual markers represent a single test conducted. Order of adhesion test presented as markers of decreasing size. Lines and gray ribbons indicate the estimated linear regression lines and 95% credible bands, respectively. The effects of test order on F_D were significant, and therefore presented as individual regression lines, and insignificant on extension at detachment and W_A so regression lines converged. Values between wet and dry treatments were significant to the right of the vertical dashed line and value presented.

where F is the applied force and A_0 is the initial cross-sectional area of the silk fiber. From the calculated stress-strain curves we were able to determine the: i) ultimate stress (MPa) and strain (mm/mm) at axial fiber breaking, ii) Young's modulus (GPa) as the initial slope of the curve from 0 to 2% strain, iii) toughness (MJ m^{-3}) as the area under the curve. These values allowed us to determine axial fiber strength, extensibility, initial resistance to deformation and work to break, respectively.

2.6. Axial fiber contraction testing

To test for a contraction response, cribellate threads were exposed to high humidity or water, as seen in other silk types such as major ampullate and flagelliform silks, following methods described by Piorkowski and Blackledge (2017). Any contraction was assumed to be attributed to the axial fibers as the cribellate fibrils were not under tension. Samples were mounted onto the tensile tester within the Perspex chamber and brought to a tension of 15 µN. Humidity was then raised from the ambient conditions of the room (45% RH, 23°C) to high humidity (>90% RH, 23°C) over a period of 60–300s. Changes in thread tension were measured over this period after which the thread was relaxed to its original tension and change in length of the thread measured (Elices et al., 2011). We found weak contraction stress (10 MPa) and shrinkage (1%) from contraction tests, however, we cannot rule out the possibility that samples were already in a maximally contracted state when collected from webs in wet environments. Nonetheless, we assumed a negligible effect of high humidity upon diameter and gauge length of the cribellate threads during tensile and adhesion testing as swelling in non-contracting spider silk fibers is generally low and difficult to measure (Gosline et al., 1984).

2.7. Modelling of scaling laws

According to the JKR adhesion model (Johnson et al., 1971) the force of detachment (F_D) is measured as:

$$F_D = 3\pi\gamma r$$

where γ is the adhesion energy and r is the effective fiber radius; the displacement at detachment is:

$$D_D=(9\pi\gamma(d/2)_{1/2}/(2E))_{2/3}$$

E being the fiber's Young modulus.

Experimental results can be rationalized for wet and dry conditions considering different adhesion energies $\gamma_{wet,dry}$ and Young's moduli $E_{wet,\,dry}$ as well as $r_{wet} = d/2$ where d is the silk thread diameter or $r_{dry} = r_0 =$ constant, i.e. a characteristic material length (e.g. axial fiber radius). The Young's modulus and especially the strength of the axial silk fibers are expected to scale (Carpinteri and Pugno, 2005) with c_i known constants, as:

$$E = c_1 E_0 d^{-m} \qquad \sigma_{MAX} = c_2 d^{-n}$$

where $0 < m,n < 1/2$ and the last limit is valid according to linear elastic fracture mechanics for the strength when assuming the defect size proportional to d, *and* E_0 is a characteristic Young modulus at an arbitrary fixed size scale. Imposing a constant ratio between the silk fracture force and the spider body weight we would expect $\sigma_{MAX} d^2$ proportional to l^D where l is the body length and D = 3 denotes the 3-dimensions of a Euclidean volume, whereas in general we thus expect the following scaling:

$$d = c3 * l_{D/(2-n)}$$

where in general 2-n < D < 3, since D = 2-n simply corresponds to *d* directly proportional to *l* and in general D is the fractal dimension of the fractal domain where the energy is dissipated (Carpinteri and Pugno, 2005).

From our model, we deduced the following scaling exponents:

$F_{D,wet} = c_3 \gamma_{wet} l_D/(2- n)$

$F_{D,dry} = c_4 \gamma_{dry}$

$D_{D,wet} = c_5 E_{-0,wet}2/3 \gamma 1_{wet}/2 l_{D(1+2m)}/(3(2- n))$

$D_{D,dry} = c_6 E_{-0,dry}2/3 \gamma 1_{dry}/2 l_{D(2m)}/(3*(2- n))$

$W_{D,wet} = c_7 E_{-0,wet}2/3 \gamma 3_{wet}/2 l_{D(4+2m)}/(3*(2- n))$

$W_{D,dry} = c_8 E_{-0,dry}2/3 \gamma 3_{dry}/2 l_{D(2m)}/(3*(2- n))$

2.8. Statistical analysis

Given that body size was scaled in this study, silk diameters were tested for an allometric relationship to spider body length among treatments to determine unexpected growth rate of a morphological trait (West et al., 1997). We performed a general linear mixed model in logarithmic form to fit silk diameter (Y_{ij}), $\log_{10}(Y_{ij}) = \beta_0 + \beta_1 \log_{10}(L) + T_j + \beta_2 T_j \log_{10}(L_i) + S_i + R_{j(i)} + \varepsilon_i$, where L denotes spider body length, T_j denotes the effect of wet/dry treatment, S_i denotes the random effect of the ith spider and $R_{j(i)}$ denotes the random effect of the ith spider identity nested within the j treatment. This model included treatment (wet = 1, dry = − 1), decimal logarithm of spider body length, and their interaction as a fixed factor/covariate. Spider identity and spider identity nested within treatment as random factors were also included according to our experimental design to account for possible pseudoreplication. We allowed residuals for each treatment with different variances (ε_i) to account for potential heteroscedasticity between dry/wet treatments. We therefore compared the scaling exponents for both treatments by testing the coefficient of interaction (β_2) = 0. Simultaneously, the scaling exponents for both treatments were estimated by $10^{(\beta 1 \pm \beta 2)}$. To test how spider body length linearly affected tensile properties (i.e. Young's modulus, engineering stress, engineering strain and toughness) we standardized properties (centered to mean = 0 and scaled to SD = 1) and then separately fit these standardized properties as dependent variables by using univariate general linear mixed models,

$\hat{Y}_{ij} = \beta_0 + \beta_1 L + T_j + \beta_2 T_j L + S_i + R_{j(i)} + \varepsilon_i.$

To test how spider body length linearly affected adhesive properties (i.e. F_D, extension and W_D), we fitted these properties with an additional effect of the test order of the adhesion tests since we repeatedly tested the adhesion of the same silk sample,

$\hat{Y}_{ijk} = \beta_0 + \beta_1 L + T_j + \beta_2 T_j L + E_k + S_i + R_{j(i)} + \varepsilon_i.$

These models included treatment (T_i; wet = 1, dry = − 1), standardized spider body length (L) and their interaction as a fixed factor/ covariate. Similarly, we also included the effect of ith spider identity (S_i) and spider identity nested within treatment [$R_{j(i)}$] as random effects. The fixed effect of kth test (E_k) in the adhesion model allow us to estimate how the test order affected adhesive properties. All models were fitted by Markov chain Monte Carlo (MCMC) techniques provided by R package 'MCMCglmm' (Hadfield, 2010). Priors for each coefficients of fixed factors/covariates were assigned to follow independent normal distributions with mean = 0 and SD = 10, and priors for each random factors/errors were assigned to follow independent inverse-gamma distributions with shape = 0.01 and scale = 0.01. These priors were uninformative and sufficient to cover our data. We performed 200,000 iterations of MCMC including the beginning 100,000 burn-in iterations in each model. After burn-in iterations, MCMC samples were thinned by gathering every 10th iteration, therefore, 10,000 MCMC iterations were used to construct the posterior distributions. Convergences of MCMC samples were visually confirmed. Autocorrelation coefficients were less than 0.05. We derived the posterior distributions of intercept, coefficient of fixed factors and covariates to estimate the credible bonds for both treatments, and then determined the significant regions (i.e. the range of spider body length with significant difference of tensile/adhesive properties between treatments) by the regions of non-overlapping credible bonds. We calculated the Bayesian coefficients of determination according to Gelman et al. (2018). Probability density distributions for all data were determined (see Fig. S1). To investigate the correlations among tensile properties and adhesive properties, we independently evaluated the Spearman's rank correlation coefficients among properties of dry and wet silks and performed exact tests. P-values were adjusted by using a Benjamini–Hochberg procedure to control for false discovery rates.

3. Results

3.1. Adhesive properties of cribellate silk

We found that exposure to high humidity did not cause matting, conglutination, or other significant structural changes to the cribellate nanofibrils (Fig. 2). Force at detachment (F_D), extension at detachment, and work of adhesion (W_A) was greater in threads exposed to high humidity (>90% RH) than lower humidity (45% RH) for all but the smallest spiders, whose silks did not differ in property when wet or dry (Fig. 3, Table 1). The increased deformation of the cribellate threads during adhesion in wet conditions compared to dry conditions was visibly apparent (Fig. 3d and e, Movie S1 & S2). The observed scalings of adhesion force, extension at detachment and work of adhesion for both wet and dry conditions are similar to the related theoretical predictions even if we assumed the intermediate values of n, $m_{dry} \sim -1/4$ and D ~9/4, noting that $m_{wet} \sim 0$ with however $E_{0,wet} \ll E_{0,dry}$. We also found that test order significantly affected F_D, but not

extension at detachment or W_A. On average, F_D decreased by 0.13 SD (~0.832 μN/mm) between the first and second tests and by 0.091 SD (~0.582 μN/mm) between second and third tests in both treatments (Fig. 3a, Table 1). The deviance information criterions (DIC) did not support the interaction between test order and treatment (ΔDIC = 3.266) or spider body length (ΔDIC = 7.728).

3.2. Tensile properties of axial fibers

Cribellate silk compliance and axial fiber extensibility were significantly affected by humidity and body size, respectively (Fig. 4, Table 2). Young's modulus decreased by around three orders of magnitude in wet conditions (0.01–0.35 GPa) compared to dry (1–8 GPa) (Fig. 4b, Table 2). Engineering strain at break increased with spider size regardless of humidity conditions (Fig. 4d, Table 2). Additionally, engineering stress at break and toughness of axial fibers was not significantly different between high and low humidity (Fig. 4, Table 2, for analysis including true stress and strain values see Fig. S2 & Table S4).

The tensile behavior of dry and wet cribellate silk threads (see Fig. 4f) exhibited typical characteristics of cribellate silk and other types of spider silk observed in other studies (see Blackledge and Hayashi, 2006a,b). We observed a strong resistance to deformation by the axial fiber, which was followed by a decreased slope of the stress-strain curve. The slope of the stress-strain curve then increased gradually until the silk experienced strain hardening whereupon the slope increased exponentially until failure. When exposed to high humidity, initial stiffness of cribellate threads decreased dramatically as the fiber softened, but maintained the other aforementioned mechanical behaviors (Fig. 4). The scaling for strength was as expected, with an intermediate value of n ~ − 1/4.

Table 1

General linear mixed model of analysis of standardized values of adhesive properties of cribellate silk tested in wet (90% RH) and dry (45% RH) conditions across body length. Values indicate posterior means and values within parentheses indicate 95% highest density intervals. Slope estimates represent standardized regression coefficients, and intercept estimates represent fitted values when spider body length are fixed at 13.35 mm † $P_{MCMC} < 0.1$; * $P_{MCMC} < 0.05$; ** $P_{MCMC} < 0.01$; *** $P_{MCMC} < 0.001$.

Property	Treatment	Intercept	Slope	Marginal R^2
Force at detachment	Dry	− 0.570 (− 0.761, − 0.368)**	0.040 (− 0.173, 0.240)	0.390 (0.242, 0.496)
	Wet	0.643 (0.266, 1.033)**	0.503 (0.129, 0.865)*	0.213 (0.059, 0.360)
	Wet vs. Dry	1.213 (0.793, 1.633)	0.463 (0.061, 0.874)*	–
	2nd test vs 1st test	− 0.130 (− 0.258, − 0.002)*	–	–
	3rd test vs 1st test	− 0.222 (− 0.356, − 0.099)***	–	–
	3rd test vs 2nd test	− 0.091 (− 0.222, 0.036)	–	–
Extension	Dry	− 0.661 (− 0.829, − 0.497)***	− 0.010 (− 0.184, 0.161)	0.373 (0.259, 0.455)
	Wet	0.759 (0.441, 1.077)***	0.556 (0.253, 0.860)***	0.256 (0.087, 0.431)
	Wet vs. Dry	1.420 (1.065, 1.763)***	0.566 (0.231, 0.902)**	–
	2nd test vs 1st test	0.010 (− 0.084, 0.105)	–	–
	3rd test vs 1st test	0.004 (− 0.093, 0.098)	–	–
	3rd test vs 2nd test	− 0.006 (− 0.100, 0.092)	–	–
Work of adhesion	Dry	− 0.611 (− 0.663, − 0.559)***	0.004 (− 0.052, 0.057)	0.497 (0.485, 0.503)
	Wet	0.687 (0.363, 1.048)***	0.634 (0.312, 0.970)***	0.250 (0.074, 0.430))
	Wet vs. Dry	1.297 (0.958, 1.641)***	0.630 (0.305, 0.965)***	–
	2nd test vs 1st test	− 0.019 (− 0.051, 0.014)	–	–
	3rd test vs 1st test	− 0.021 (− 0.055, 0.010)	–	–
	3rd test vs 2nd test	− 0.002 (− 0.036, 0.029)	–	–

3.3. Interaction between tensile and adhesive properties

We found a significant correlation between Young's modulus and extension at detachment in the wet silks ($p = 0.045$ after a Benjamini–Hochberg adjustment, see Fig. S3). There were no significant correlations between variables for the dry silks. The interaction between fracture strength (σ_{MAX}) and adhesion strength ($\sigma_D = F_D/d^2$) is evident (noting that from the previous scaling laws $\sigma_D \propto \sigma^{p/n}{}_{MAX}$, where $p = 1,2$ for wet or dry adhesion respectively).

4. Discussion

Our results supported our expectation that mechanical plasticization

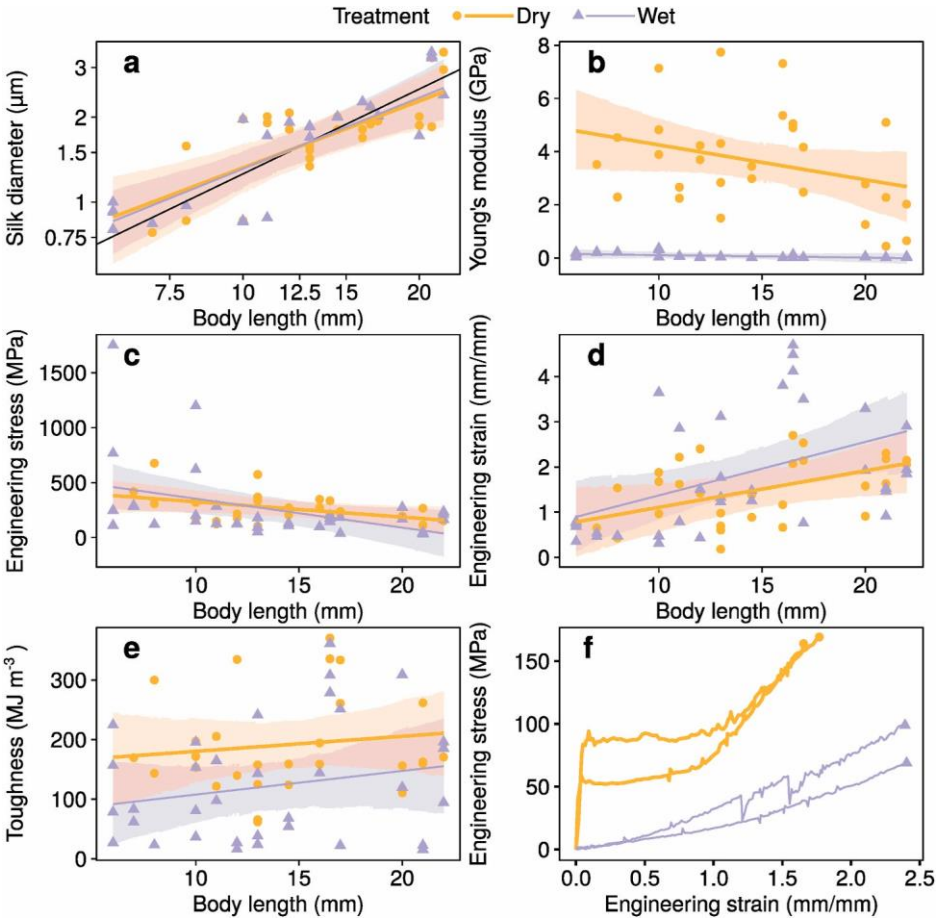

Fig. 4. Axial fiber diameters (a), tensile properties, including engineering stress and strain at breaking (b–e) and representative tensile behavior (f) of *H. troglodytes* cribellate capture silk in relation to body length and exposure treatment (Dry: 45% RH, Wet: 90% RH). Individual markers represent a single test conducted. Lines and gray ribbons indicate the estimated linear regression lines and 95% confidence bands, respectively. Black line in (a) represents a slope of isometry (slope = 1). Representative tensile curves were taken from four silk samples, two each from two individuals.

of axial fibers by atmospheric water can improve work of adhesion of cribellate silk threads. Unexpectedly, however, this effect appears to have been enhanced in silk threads from increasingly larger spiders with no effect observed in very small individuals (Fig. 3, Table 1). We speculate this may be due to increased efficiency of energy dissipation from adhesive nanofibril to axial fiber, possibly due to differences in diametrical change under loading, and/or a greater number of contact points of the cribellate nanofibrils to the substrate resulting from an increase in number of spigots on the cribellum across ontogenetic development (Opell, 1995; Alfaro et al., 2018). Further investigation is needed to confirm. Nonetheless, our findings highlight a previously undescribed mechanism involving the axial fiber implicit in improving adhesion under high humidity and add to a growing body of work in describing the adhesive mechanisms of this system.

Previous work by Hawthorn and Opell (2002; 2003) demonstrated increases in adhesive force of cribellate silk at high humidity in several species of spider. Hygroscopic and van der Waals forces are indicated to be the driving mechanisms generating adhesion and are likely enhanced by high humidity, forming stronger attachment points along a substrate. In this study, our results do not refute this hypothesis as we also observe increased F_D with increased humidity (Fig. 3a, Table 1). However, these previous studies did not take into account the potential influence of humidity upon mechanical properties of the axial fiber.

We observed that when the cribellate silk was dry the work of adhesion was performed primarily by the cribellate nanofibrils (Movie S1). This supports the hypothesis that the dry axial fibers are too stiff to deform in a way that contributes to adhesion (Hawthorn and Opell, 2002; Blackledge and Hayashi, 2006a; Sahni et al., 2011). The force of detachment for the cribellate nanofibrils that we measured (i.e. 10–124 µN) was achieved by the accompanying axial fibers after less than 1% strain (ln (mm/mm)). When wet, however, the softened axial fibers are capable of stretching 10–20% of their original length before reaching F_D. While it is possible that wetting also softened the nanofibrils, allowing them to extend further than when dry and "flow" better along a surface, we did not detect any structural indicators of this. We also found a significant negative correlation between Young's modulus and the extension at detachment when wet, but not when dry (Fig. S3). These results indicate stretching of the more compliant axial fiber during adhesion in high humidity, which we interpret as the axial fiber performing some work of adhesion.

Water is a known plasticizer of many silks (Gosline et al., 1984; Shao et al., 1999; Plaza et al., 2008; Bauer et al., 2012; Guinea et al., 2012; Piorkowski et al., 2018a,b). Compliance and extensibility are a result of water penetrating the silk fibers' internal structure and disrupting the hydrogen bonds between protein chains, allowing for greater molecular mobility (Termonia, 1994; Jelinski et al., 1999; Perez-Rigueiro et al., ´ 2003). The Young's modulus of cribellate silks measured for medium to large sized *H. troglodytes* (body length > 11 mm) ranged from 0.13 to 0.009 GPa, and engineering strain ranged from 1.0 to 2.1 (mm/mm). These values fall within the range of what has been observed for the flagelliform threads of derived orb web spiders, which are known for their high compliance

(Young's modulus: 0.01–0.001 GPa) and extensibility (engineering strain: 0.7–4.4 (mm/mm; Swanson et al., 2007). Given these similarities, cribellate silk thread adhesion in high humidity could operate similar to that of viscid silk, with some mechanical work transferred to the axial fiber. It appears that compliance in supporting fibers in silk-based adhesive systems is emerging as an important property that contributes to the overall work of adhesion through deformation at small forces (Meyer et al., 2014; Guo et al., 2018).

The enhanced, rather than disrupted, adhesive strength of cribellate

Table 2

General linear mixed model of analysis of standardized values of tensile properties of cribellate silk tested in wet (90% RH) and dry (45% RH) conditions across body length. Values indicate posterior means and values within parentheses indicate 95% highest density intervals. Slope estimates represent standardized regression coefficients, and intercept estimates represent fitted values when spider body length are fixed at 12.63 mm † $P_{MCMC} < 0.1$; * $P_{MCMC} < 0.05$; ** $P_{MCMC} < 0.01$; *** $P_{MCMC} < 0.001$.

Property	Treatment	Intercept	Slope	Marginal R^2
Diameter	Dry	− 0.665 (− 1.115, − 0.221)**	0.787 (0.384, 1.161)**	0.535 (0.243, 0.733)
	Wet	− 0.719 (− 1.066, − 0.355)**	0.837 (0.516, 1.170)***	0.640 (0.410, 0.769)
	Wet vs. Dry	− 0.054 (− 0.487, 0.391)	0.051 (− 0.338, 0.428)	–
Young's modulus	Dry	0.955 (0.634, 1.293)***	− 0.295 (− 0.651, 0.046)†	0.165 (<0.001, 0.384)
	Wet	− 0.777 (− 0.824, − 0.732)***	− 0.021 (− 0.063, 0.022)	0.354 (0.004, 0.630)
	Wet vs. Dry	− 1.732 (− 2.051, − 1.390)***	0.274 (− 0.103, 0.595)	–
Engineering stress	Dry	0.102 (− 0.235, 0.437)	− 0.304 (− 0.622, − 0.007)*	0.123 (<0.001, 0.313)
	Wet	0.026 (− 0.462, 0.524)	− 0.574 (− 1.063, − 0.122)**	0.045 (<0.001, 0.130)
	Wet vs. Dry	− 0.076 (− 0.618, 0.481)	− 0.270 (− 0.806, 0.247)	–
Engineering strain	Dry	− 0.258 (− 0.672, 0.144)	0.383 (0.029, 0.738)*	0.144 (<0.001, 0.446)
	Wet	0.134 (− 0.333, 0.559)	0.561 (0.144, 0.971)**	0.080 (<0.001, 0.265)
	Wet vs. Dry	0.392 (− 0.162, 0.932)	0.178 (− 0.337, 0.680)	
Toughness	Dry	0.438 (− 0.087, 0.916)†	0.151 (− 0.331, 0.618)	0.076 (<0.001, 0.239)
	Wet	− 0.402 (− 0.904, 0.087)	0.238 (− 0.233, 0.693)	0.096 (<0.001, 0.282)
	Wet vs. Dry	− 0.839 (− 1.459, − 0.231)*	0.087 (− 0.525, 0.682)	–

silk of *H. trogoldytes* in high humidity is unsurprising as these animals spend much of their lifetimes in wet environments (Doran et al., 1999; Piorkowski et al., 2018a). This observation may indicate an evolutionary adaptation of this species that promotes greater foraging capabilities, although further investigations are needed. This study is a part of a growing body of evidence that suggests mechanical plasticization of underlying components of biological adhesives by water is one mechanism responsible for increased adhesion at high humidity. Examples include gecko foot setae (Puthoff et al., 2010) and gluey spider and insect capture silk threads (Meyer et al., 2014; Guo et al., 2018; Piorkowski et al., 2018b). Further examining these unique polymeric bioadhesives opens a pathway toward the development of synthetic adhesives that can be softened and plasticized while retaining mechanical and adhesive integrity.

5. Conclusions

We herein demonstrated that increasing compliance through exposure to high humidity of the underlying axial fibers of the cribellate silk threads of *H. troglodytes* improves work of adhesion. We showed that the axial fiber likely plays a key role in adhesion by performing work during peel off from a substrate. Our results, rationalized with theoretical scaling laws, highlight a novel function of cribellate axial fibers in generating adhesion. Design of future synthetic materials that need to perform in wet environments could draw inspiration from how atmospheric water facilitates, rather than diminishes, cribellate silk adhesion.

Funding

Research was funded by Ministry of Science and Technology, Taiwan, grants (MOST 108-2811-B-029-500) to DP and (MOST 106- 2311-B-029-003-MY3) to IMT, the Deutsche Forschungsgemeinschaft grant (DFG, JO 1464/1-1) to ACJ, a Hermon Slade Foundation grant (HSF17/6) to SJB and NMP is supported by the European Commission under FET Proactive 'Neurofibres' grant no. 732344, as well as by the Italian Ministry of Education, University and Research (MIUR) under the 'Departments of Excellence' grant L. 232/2016 and AR 901–01384—PROSCAN and PRIN-20177TTP3S.

Author Statement

Dakota Piorkowski: Conceptualization, Methodology, Investigation, Writing - original draft, Writing - review & editing. Chen-Pan Liao: Visualization, Formal analysis, Writing - review & editing. Anna- Christin Joel: Methodology, Investigation, Writing - review & editing. Chung-Lin Wu: Resources, Visualization. Niall Doran: Methodology. Sean J. Blamires: Methodology, Writing - review & editing. Nicola M. Pugno: Methodology, Writing - review & editing. I-Min Tso: Conceptualization, Funding acquisition, Writing - review & editing.

Declaration of competing interest

The authors declare that they have no known competing financial interests or personal relationships that could have appeared to influence the work reported in this paper.

Acknowledgements

We thank Hamish Craig, Xungai Wang, and Jian Fang for assistance during field collections, and Todd Blackledge and Fritz Vollrath for feedback during the writing of the original manuscript.

Appendix A. Supplementary data

Supplementary data to this article can be found online at https://doi.org/10.1016/j.jmbbm.2020.104200.

References

Alfaro, R.E., Griswold, C.E., Miller, K.B., 2018. The ontogeny of the spinning apparatus of Tengella perfuga (Araneae: zoropsidae). Invertebr. Biol. 137, 187–204.
Bascom, W.D., 1974. The surface chemistry of moisture-induced composite failure. In: Plueddemann (Ed.), Interfaces in Polymer Matrix Composites, pp. 79–108.
Bauer, F., Bertinetti, L., Masic, A., Scheibel, T., 2012. Dependence of mechanical properties of lacewing egg stalks on relative humidity. Biomacromolecules 13, 3730–3735.
Blackledge, T.A., Hayashi, C.Y., 2006a. Unraveling the mechanical properties of composite silk threads spun by cribellate orb-weaving spiders. J. Exp. Biol. 209, 3131–3140.
Blackledge, T.A., Hayashi, C.Y., 2006b. Silken toolkits: biomechanics of silk fibers spun by the orb web spider Argiope argentata (Fabricius 1775). J. Exp. Biol. 209, 2452–2461.
Blackledge, T.A., Cardullo, R.A., Hayashi, C.Y., 2005. Polarized light microscopy, variability in spider silk diameters, and the mechanical characterization of spider silk. Invertebr. Biol. 124, 165–173.
Blackledge, T.A., Kuntner, M., Agnarsson, I., 2011. The form and function of spider orb webs: evolution from silk to ecosystems. Adv. Insect Physiol 41, 175–262.
Bott, R.A., Baumgartner, W., Braunig, P., Menzel, F., Joel, A.C., 2017. Adhesion¨ enhancement of cribellate capture threads by epicuticular waxes of the insect prey sheds new light on spider web evolution. P. Roy. Soc. B. 284, 20170363.
Carpinteri, A., Pugno, N., 2005. Are the scaling laws on strength of solids related to mechanics or to geometry? Nat. Mater. 4, 421–423.
Doran, N.E., Kiernan, K., Swain, R., Richardson, A.M., 1999. Hickmania troglodytes, the Tasmanian cave spider, and its potential role in cave management. J. Insect Conserv. 3, 257–262.
Eberhard, W.G., 1988. Combing and sticky silk attachment behaviour by cribellate spiders and its taxonomic implications. Bull. Br. Arachnol. Soc. 7, 247–251.
Eberhard, W.G., 1990. Function and phylogeny of spider webs. Annu. Rev. Ecol. Systemat. 21, 341–372.
Eberhard, W., Pereira, F., 1993. Ultrastructure of cribellate silk of nine species in eight families and possible taxonomic implications (araneae: amaurobiidae, deinopidae, desidae, dictynidae, filistatidae, hypochilidae, stiphidiidae, tengellidae). J. Arachnol. 21, 161–174.
Elettro, H., Neukirch, S., Antkowiak, A., Vollrath, F., 2015. Adhesion of dry and wet electrostatic capture silk of uloborid spider. Sci. Nat. 102, 41.
Elices, M., Plaza, G.R., P´erez-Rigueiro, J., Guinea, G.V., 2011. The hidden link between supercontraction and mechanical behavior of spider silks. J. Mech. Behav. Biomed. Mater. 4, 658–669.
Gelman, A., Goodrich, B., Gabry, J., Vehtari, A., 2018. R-squared for Bayesian regression models. Am. Statistician 73, 307–309.
Gosline, J.M., Denny, M.W., DeMont, M.E., 1984. Spider silk as rubber. Nature 309, 551–552.
Guinea, G.V., Elices, M., Plaza, G.R., Perea, G.B., Daza, R., Riekel, C., Agullo-Rueda, F.,´ Hayashi, C., Zhao, Y., Perez-Rigueiro, J., 2012. Minor ampullate silks from Nephila´ and Argiope spiders: tensile properties and microstructural characterization. Biomacromolecules 13, 2087–2098.
Guo, Y, Chang, Z, Guo, HY, Fang, W, Li, QY, Zhao, HP, Feng, XQ, Gao, H, 2018. Synergistic adhesion mechanismsof spider capture silk. J. R. Soc. Interface 15, 20170894. https://doi.org/10.1098/rsif.2017.0894.
Hadfield, J., 2010. MCMC methods for multi-response generalized linear mixed models: the MCMCglmm R package. J. Stat. Software 33, 1–22.
Hawthorn, A.C., Opell, B.D., 2002. Evolution of adhesive mechanisms in cribellar spider prey capture thread: evidence for van der Waals and hygroscopic forces. Biol. J. Linn. Soc. 77, 1–8.
Hawthorn, A.C., Opell, B.D., 2003. van der Waals and hygroscopic forces of adhesion generated by spider capture threads. J. Exp. Biol. 206, 3905–3911.
Higgins, E.T., Petterd, W.F., 1883. Description of a new cave-inhabiting spider, together with notes on mammalian remains from a recently discovered cave in the Chudleigh district. Pap. Proc. Roy. Soc. Tasmania 1882, 191–192.
Ito, S., Hashimoto, M., Wadgaonkar, B., Svizero, N., Carvalho, R.M., Yiu, C., Rueggeberg, F.A., Foulger, S., Saito, T., Nishitani, Y., Yoshiyama, M., Yoshiyama, M., Tay, F.R., Pashley, D.H., 2005. Effects of resin hydrophilicity on water sorption and changes in modulus of elasticity. Biomaterials 26, 6449–6459.
Jelinski, L.W., Blye, A., Liivak, O., Michal, C., LaVerde, G., Seidel, A., Shah, N., Yang, Z., 1999. Orientation, structure, wet-spinning, and molecular basis for supercontraction of spider dragline silk. Int. J. Biol. Macromol. 24, 197–201.
Joel, A.C., Baumgartner, W., 2017. Nanofibre production in spiders without electric charge. J. Exp. Biol. 220, 2243–2249.

Joel, A.C., Kappel, P., Adamova, H., Baumgartner, W., Scholz, I., 2015. Cribellate thread production in spiders: complex processing of nano-fibres into a functional capture thread. Arthropod Struct. Dev. 44, 568–573.
Johnson, K.L., Kendall, K., Roberts, A.D., 1971. Surface energy and the contact of elastic solids. Proc. Roy. Soc. Lond. A 324, 301–313.
Kovoor, J., 1987. Comparative structure and histochemistry of silk-producing organs in arachnids. In: Nentwig, W. (Ed.), Ecophysiology of Spiders. Springer, Berlin, pp. 160–186.
Kronenberger, K., Vollrath, F., 2015. Spiders spinning electrically charged nano-fibres. Biol. Lett. 11, 20140813.
Lee, L.H., 2013. Fundamentals of Adhesion. Springer Science & Business Media.
Liao, X., Yin, G., Huang, Z., Yao, Y., Gu, J., Han, D., 2011. Supercontraction on cribellate spider spiral silk with wet-rebuilt micro-structure. Mater. Sci. Eng. C 31, 128–133.
Lopardo, L., Ramírez, M.J., Grismado, C., Compagnucci, L.A., 2004. Web building behavior and the phylogeny of austrochiline spiders. J. Arachnol. 32, 42–54.
Marom, G., 1985. The role of water transport in composite materials. In: Comyn, J. (Ed.), Polymer Permeability, Chap. 9. Elsevier Applied Science Publishers, New York, USA, pp. 341–374.
Meyer, A., Pugno, N.M., Cranford, S.W., 2014. Compliant threads maximize spider silk connection strength and toughness. J. Roy. Soc. Interface 11, 20140561.
Musto, P., Ragosta, G., Scarinzi, G., Mascia, L., 2002. Probing the molecular interactions in the diffusion of water through epoxy and epoxy–bismaleimide networks. J. Polym. Sci., Polym. Phys. Ed. 40, 922–938.
Opell, B.D., 1995. Ontogenetic changes in cribellum spigot number and cribellar prey capture thread stickiness in the spider family Uloboridae. J. Morphol. 224, 47–56.
Opell, B.D., Hendricks, M.L., 2007. Adhesive recruitment by the viscous capture threads of araneoid orb-weaving spiders. J. Exp. Biol. 210, 553–560.
Perea, G.B., Riekel, C., Guinea, G.V., Madurga, R., Daza, R., Burghammer, M., Hayashi, C., Elices, M., Perez-Rigueiro, J., 2013. Identification and dynamics of´ polyglycine II nanocrystals in Argiope trifasciata flagelliform silk. Sci. Rep. 3, 1–6.
Perez-Rigueiro, J., Elices, M., Guinea, G.V., 2003. Controlled supercontraction tailors the´ tensile behaviour of spider silk. Polymer 44, 3733–3736.
Piorkowski, D., Blackledge, T.A., 2017. Punctuated evolution of viscid silk in spider orb webs supported by mechanical behavior of wet cribellate silk. Sci. Nat. 104, 67. Piorkowski, D., Blamires, S.J., Doran, N.E., Liao, C.P., Wu, C.L., Tso, I.M., 2018a. Ontogenetic shift toward stronger, tougher silk of a web-building, cave-dwelling spider. J. Zool. 304, 81–89.
Piorkowski, D., Blackledge, T.A., Liao, C.P., Doran, N.E., Wu, C.L., Blamires, S.J., Tso, I. M., 2018b. Humidity-dependent mechanical and adhesive properties of Arachnocampa tasmaniensis capture threads. J. Zool. 305, 256–266.
Plaza, G.R., Guinea, G.V., Perez-Rigueiro, J., Elices, M., 2006. Thermo-hygro-mechanical´ behavior of spider dragline silk: glassy and rubbery states. J. Polym. Sci., Polym. Phys. Ed. 44, 994–999.
Plaza, G.R., Corsini, P., P´erez-Rigueiro, J., Marsano, E., Guinea, G.V., Elices, M., 2008. Effect of water on Bombyx mori regenerated silk fibers and its application in modifying their mechanical properties. J. Appl. Polym. Sci. 109, 1793–1801.
Puthoff, J.B., Prowse, M.S., Wilkinson, M., Autumn, K., 2010. Changes in materials properties explain the effects of humidity on gecko adhesion. J. Exp. Biol. 213, 3699–3704.
Sahni, V., Blackledge, T.A., Dhinojwala, A., 2011. A review on spider silk adhesion. J. Adhes. 87, 595–614.
Sahni, V., Miyoshi, T., Chen, K., Jain, D., Blamires, S.J., Blackledge, T.A., Dhinojwala, A., 2014. Direct solvation of glycoproteins by salts in spider silk glues enhances adhesion and helps to explain the evolution of modern spider orb webs. Biomacromolecules 15, 1225–1232.
Shao, Z., Young, R.J., Vollrath, F., 1999. The effect of solvents on spider silk studied by mechanical testing and single-fibre Raman spectroscopy. Int. J. Biol. Macromol. 24, 295–300.
Swanson, B.O., Blackledge, T.A., Hayashi, C.Y., 2007. Spider capture silk: performance implications of variation in an exceptional biomaterial. J. Exp. Zool. Part A 307, 654–666.
Termonia, Y., 1994. Molecular modeling of spider silk elasticity. Macromolecules 27, 7378–7381.
Vollrath, F., Edmonds, D.T., 1989. Modulation of the mechanical properties of spider silk by coating with water. Nature 340, 305–310.
West, G.B., Brown, J.H., Enquist, B.J., 1997. A general model for the origin of allometric scaling laws in biology. Science 276, 122–126.
Wolff, E.G., 1993. Moisture effects on polymer matrix composites. SAMPE J. 29, 11–19.
Wolff, J.O., Wells, D., Reid, C.R., Blamires, S.J., 2017. Clarity of objectives and working principles enhances the success of biomimetic programs. Bioinspiration Biomimetics 12, 051001.

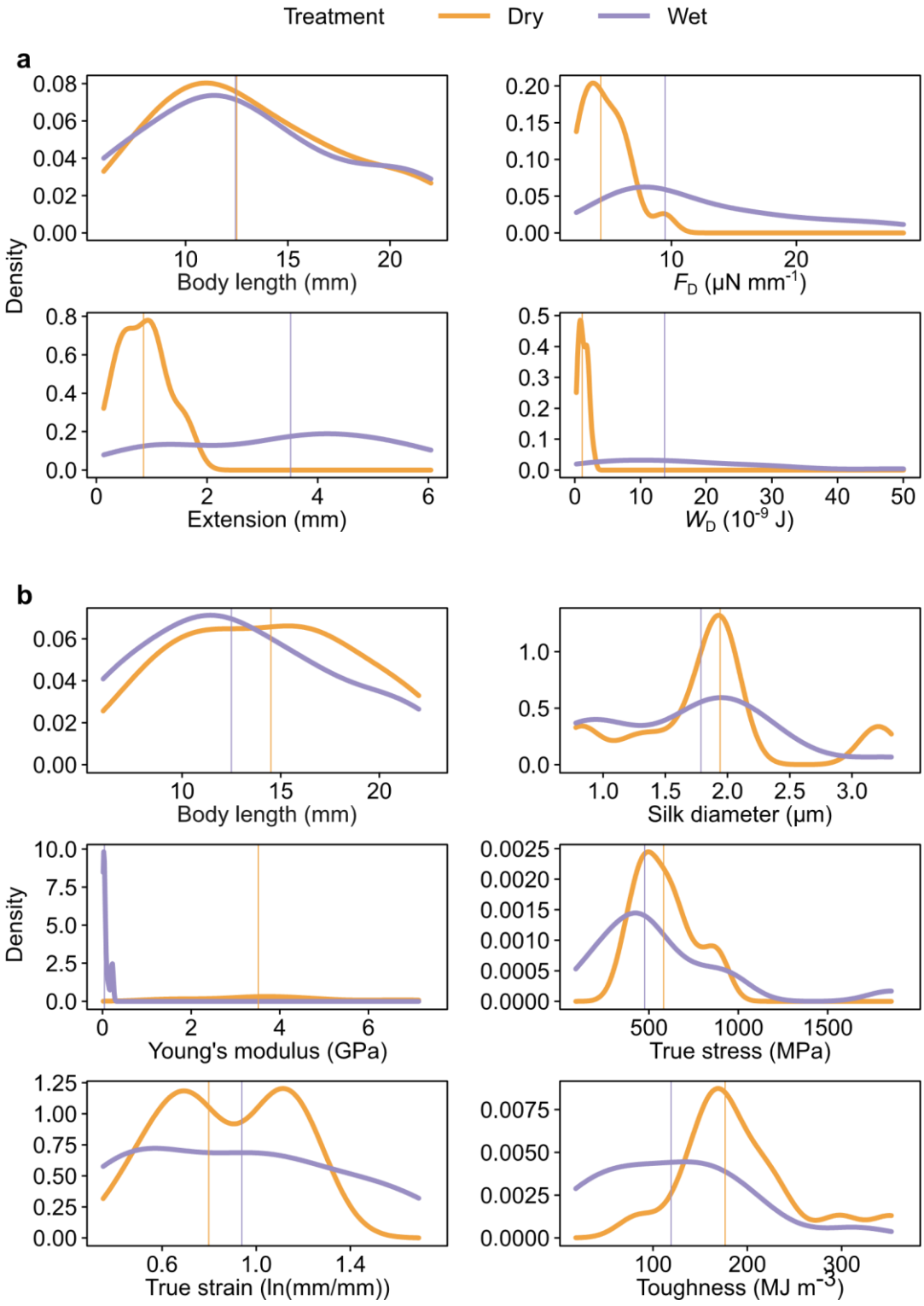

Fig. S1 – Probability density distributions of adhesive (a) and tensile (b) properties in dry and wet conditions estimated by the kernel density estimation. The vertical lines represent medians.

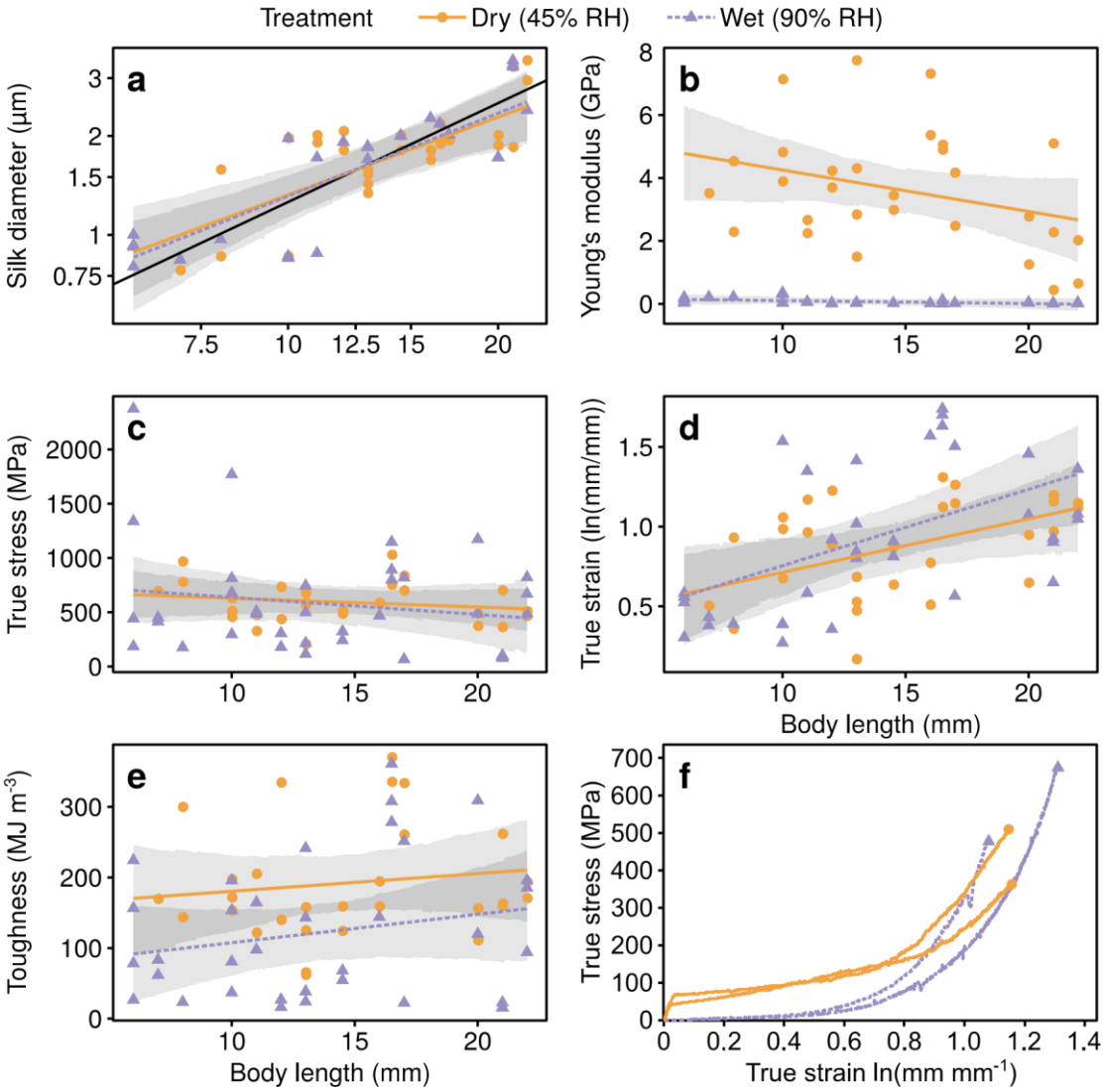

Fig. S2 – Axial fiber diameters (a), tensile properties (b-e) and representative tensile behavior (f) of *H. troglodytes* cribellate capture silk in relation to body length and exposure treatment (Dry: 45% RH, Wet: 90% RH). True values for breaking stress and strain used. Individual markers represent a single test conducted. Lines and gray ribbons indicate the estimated linear regression lines and 95% confidence bands, respectively. Black line in (a) represents a slope of isometry (slope = 1). Representative tensile curves were taken from four silk samples, two each from two individuals.

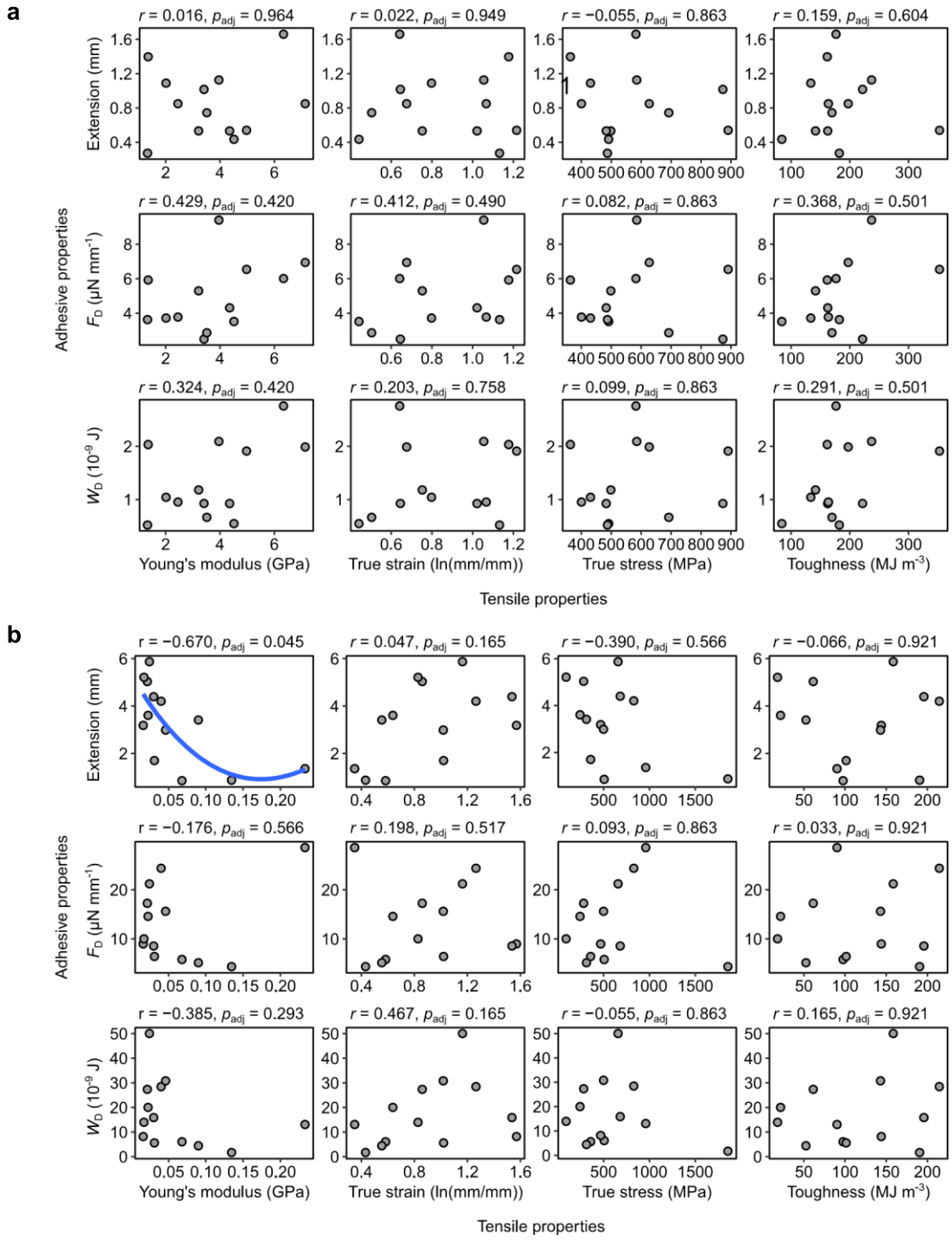

Fig. S3 – Scatter plots of adhesive properties against tensile properties of cribellate silk from averaged data of *N* = 13 individuals of *H. troglodytes* tested in dry (a) and wet (b) conditions. A significant correlation between adhesive extension and Young's modulus was detected and the blue line represents

the locally estimated scatterplot smoothing (LOESS) lines showing the negative correlation. *r* indicate Spearman's rank correlation coefficient, and the p_{adj} indicate the adjusted *p*-values.

Table S1 – Number of spiders used in adhesion and tensile tests. Values within parentheses indicate the total numbers of tests in adhesion testing and the total silk samples tested in tensile tests.

Testing property	Treatment	Body length (mm)					
		6-9	9-12	12-15	15-18	18-21	21-24
Adhesion	Dry	3 (9)	6 (18)	3 (8)	3 (9)	2 (6)	1 (3)
Adhesion	Wet	1 (3)	5 (15)	3 (9)	2 (5)	2 (6)	1 (2)
Tensile	Dry	2 (3)	4 (7)	2 (6)	4 (6)	2 (5)	1 (2)
Tensile	Wet	2 (3)	5 (8)	3 (6)	3 (6)	2 (5)	1 (3)

Table S4 – General linear mixed model of analysis of standardized values of tensile properties of cribellate silk tested in wet (90% RH) and dry (45% RH) conditions across body length. Values indicate posterior means and values

within parentheses indicate 95% highest density intervals. Slope estimates represent standardized regression coefficients, and intercept estimates represent fitted values when spider body length are fixed at 13.35 mm. † $P_{MCMC} < 0.1$; * $P_{MCMC} < 0.05$; ** $P_{MCMC} < 0.01$; *** $P_{MCMC} < 0.001$.

Property	Treatment	Intercept	Slope	Marginal R^2
Diameter	Dry	−0.666 (−1.157, −0.246)**	0.787 (0.414, 1.205)***	0.535 (0.242, 0.733)
	Wet	−0.721 (−1.069, −0.360)**	0.839 (0.514, 1.163)***	0.642 (0.420, 0.769)
	Wet vs. Dry	−0.055 (−0.520, 0.380)	0.052 (−0.340, 0.456)	—
Young's modulus	Dry	0.955 (0.643, 1.305)***	−0.296 (−0.653, 0.034)†	0.165 (< 0.001, 0.387)
	Wet	−0.777 (−0.822, −0.730)***	−0.021 (−0.065, 0.022)	0.356 (0.004, 0.630)
	Wet vs. Dry	−1.732 (−2.077, −1.411)***	0.275 (−0.068, 0.617)	—
True stress	Dry	0.074 (−0.285, 0.442)	−0.124 (−0.434, 0.218)	0.111 (< 0.001, 0.342)
	Wet	0.012 (−0.548, 0.549)	−0.242 (−0.782, 0.257)	0.067 (< 0.001, 0.210)
	Wet vs. Dry	−0.062 (−0.637, 0.572)	−0.118 (−0.717, 0.454)	—
True strain	Dry	−0.186 (−0.618, 0.248)	0.443 (0.030, 0.828)*	0.291 (< 0.001, 0.502)
	Wet	0.072 (−0.349, 0.519)	0.633 (0.249, 1.060)**	0.292 (0.063, 0.512)
	Wet vs. Dry	0.258 (−0.304, 0.803)	0.190 (−0.305, 0.754)	—
Toughness	Dry	0.439 (−0.065, 0.936)†	0.151 (−0.306, 0.646)	0.077 (< 0.001, 0.242)
	Wet	−0.402 (−0.880, 0.114)	0.241 (−0.183, 0.744)	0.096 (< 0.001, 0.288)
	Wet vs. Dry	−0.840 (−1.432, −0.215)*	0.091 (−0.477, 0.727)	—